Considerable Model–Data Mismatch in Temperature over China during the Mid-Holocene: Results of PMIP Simulations

DABANG JIANG

Nansen-Zhu International Research Centre, Institute of Atmospheric Physics, and Key Laboratory of Regional Climate-Environment Research for Temperate East Asia, and Climate Change Research Center, Chinese Academy of Sciences, Beijing, China

XIANMEI LANG

International Center for Climate and Environment Sciences, Institute of Atmospheric Physics, Chinese Academy of Sciences, Beijing, China

ZHIPING TIAN

Nansen-Zhu International Research Centre, Institute of Atmospheric Physics, and Graduate University of Chinese Academy of Sciences, Beijing, China

TAO WANG

Nansen-Zhu International Research Centre, Institute of Atmospheric Physics, Chinese Academy of Sciences, Beijing, China

(Manuscript received 16 February 2011, in final form 8 January 2012)

ABSTRACT

Using the experiments undertaken by 36 climate models participating in the Paleoclimate Modeling Intercomparison Project (PMIP), this study examines annual and seasonal surface temperatures over China during the mid-Holocene. Compared to the present or preindustrial climate, 35 out of the 36 PMIP models reproduced colder-than-baseline annual temperature, with an average cooling of 0.4 K, during that period. Seasonal temperature change followed closely the change in incoming solar radiation at the top of the atmosphere over China during the mid-Holocene. Temperature was reduced (elevated) in boreal winter and spring (summer) in all of the PMIP models, with an average of 1.4 K (1.0 K) at the national scale. Colder (warmer)-than-baseline temperatures were derived from 14 of the 16 atmosphere-only (18 of the 20 coupled) models during the mid-Holocene boreal autumn. Interactive ocean was found to lead to a warming effect on annual (0.3 K), boreal winter (0.5 K), and boreal autumn (0.7 K) temperatures, with reference to the atmosphere-only models. Interactive vegetation had little impact in terms of six pairs of coupled models with and without vegetation effects. The above results are in stark contrast to warmer-than-present annual and winter climate conditions as derived from multiproxy data for the mid-Holocene. Coupled models generally perform better than atmosphere-only models.

1. Introduction

The mid-Holocene was around 6000 yr before present, when the climate and environment differed significantly from the present day. Much effort has been devoted to investigating the response of climate models to the different seasonal distribution of incoming insolation due to changes in the earth's orbital parameters during the mid-Holocene. In particular, model–model and model–data comparisons have been widely performed to identify and understand the consistencies and inconsistencies between each other.

A few simulations of the mid-Holocene climate over China have been conducted using atmospheric general circulation models (AGCMs) (Wang 1999, 2000, 2002; Chen et al. 2002), regional climate models nested within AGCMs (Zheng et al. 2004; Liu et al. 2010a), an asynchronously coupled atmosphere–ocean general circulation model (Wei and Wang 2004), and a synchronously

Corresponding author address: Dr. Dabang Jiang, Institute of Atmospheric Physics, Chinese Academy of Sciences, P.O. Box 9804, Beijing 100029, China.
E-mail: jiangdb@mail.iap.ac.cn

DOI: 10.1175/JCLI-D-11-00231.1

coupled atmosphere–ocean general circulation model (AOGCM) (Zheng and Yu 2009). Surface warming and the intensification of monsoon circulation over China during the mid-Holocene summer (June–August) have been well documented in those earlier studies. However, both the spatial pattern and the magnitude of summer climate change are different among those simulations. Such model-dependent results imply a large degree of uncertainty in the summer climate over China during the mid-Holocene, particularly at the subregional scale, which stresses the need to investigate the mid-Holocene summer climate from the perspective of multiple climate models. Second, little or no attention has hitherto been paid to climate change for the annual mean and the other seasons during that period. Based on a variety of proxy data, Chinese climate has been found to undergo dramatic changes during the mid-Holocene. Among these includes an annual temperature increase of 1–5 K and a warmer winter (December–February), with respect to the present day (see section 4 of this study). Compared to the proxy data, the extent to which annual and seasonal temperatures over China respond to the mid-Holocene forcings in the climate models remains an open question. Previously, Chen et al. (2002) used an AGCM to reproduce a colder-than-present winter temperature of around 2.0 K over China for the mid-Holocene, which was opposite in sign to the proxy data. Investigating how winter temperature changed during that period by the use of multiple climate models is particularly interesting. Third, ocean and vegetation dynamics are typically neglected in most of the earlier simulations for the East Asian climate during the mid-Holocene. It is therefore important to examine what the Chinese climate was like during that period in the simulations of state-of-the-art AOGCMs and fully coupled atmosphere–ocean–vegetation general circulation models (AOVGCMs).

Within the framework of the Paleoclimate Modeling Intercomparison Project (PMIP), a hierarchy of climate models has been used to simulate the mid-Holocene climate. Their results have been compared to proxy data in the tropics (Braconnot et al. 2007a), Africa (Peyron et al. 2006), Europe (Guiot et al. 1999; Masson et al. 1999; Bonfils et al. 2004; Hoar et al. 2004), the high northern latitudes (Zhang et al. 2010), and Greenland and Antarctica (Masson-Delmotte et al. 2006). It is found that climate models are able to reproduce many of the robust qualitative large-scale features of reconstructed climate change, consistent with our understanding of orbital forcing (Jansen et al. 2007). Recently, the mid-Holocene warmer summer climate in East Asia was obtained from 12 AOGCMs within the second stage of the PMIP (PMIP2), which was found to generally agree with annually resolved records at 19 sites over China (Wang et al. 2010). However, such a comparison between summer temperature in the models and the annual mean for the proxy data is not matched. A fair model–data comparison should be annual versus annual and summer versus summer. The spatial coverage of the proxy data is also extremely sparse across the country. Additionally, Wang et al. only used part of the PMIP2 AOGCMs, which makes it impossible to evaluate the role of the ocean and vegetation through the comparison of the different PMIP sets of simulations. Taken together, of special interest now are the questions regarding the degree to which the mid-Holocene annual and seasonal temperatures as derived from all of the PMIP models are consistent with proxy data over China, and the degree to which interactive vegetation and ocean impact the mid-Holocene climate over this region. It is also equally important to quantify the spread of the temperature change over China from the PMIP simulations. Insights gained from this regional-scale case study will contribute to a global perspective concerning model–data comparisons during the mid-Holocene, as such a comparison between multiple climate models and proxy data is still absent in the scientific literature.

2. Data

a. Models and data

This study is based on all of the available simulations for the mid-Holocene in the PMIP, including experiments using 16 AGCMs from the first stage of the PMIP (PMIP1) and 14 AOGCMs and 6 AOVGCMs from the PMIP2. For the mid-Holocene experiment, the most important change in boundary conditions is the change in the earth's orbital parameters, which intensifies (weakens) the seasonal distribution of the incoming solar radiation at the top of the atmosphere in the Northern (Southern) Hemisphere, by about 5% (Berger 1978). In addition, atmospheric CO_2 concentration varies from 345 ppm for the present period to 280 ppm for the mid-Holocene in the PMIP1. In the PMIP2, atmospheric CO_2 concentration is held constant at 280 ppm, while atmospheric CH_4 concentration is set to 760 ppb for the preindustrial period and 650 ppb for the mid-Holocene. Sea surface temperatures (SSTs) are fixed at the present-day values in all the experiments of the 16 AGCMs in the PMIP1, while they are computed by oceanic general circulation models in all the experiments of the 20 AOGCMs and AOVGCMs in the PMIP2. All other conditions are kept constant throughout the experiments in the PMIP1 and PMIP2 simulations. Basic information about these 36 climate models

TABLE 1. Basic information on the general circulation models in the PMIP.

	Model ID	Project	Atmospheric resolution	Length of run analyzed (yr)	Baseline period
1	CCC2.0	PMIP1 (AGCM)	T32L10	10	Modern
2	CCM3	PMIP1 (AGCM)	T42L18	8	Modern
3	CCSR1	PMIP1 (AGCM)	T21L20	10	Modern
4	Centre National de Recherches Météorologiques-2 (CNRM-2)	PMIP1 (AGCM)	T31L19	10	Modern
5	CSIRO	PMIP1 (AGCM)	R21L9	15	Modern
6	ECHAM3	PMIP1 (AGCM)	T42L19	10	Modern
7	Global Environmental and Ecological Simulation of Interactive Systems (GENESIS) version 2 (GEN2)	PMIP1 (AGCM)	T31L18	10	Modern
8	Geophysical Fluid Dynamics Laboratory (GFDL)	PMIP1 (AGCM)	R30L20	25	Modern
9	Goddard Institute for Space Studies Model II (GISS-IIP)	PMIP1 (AGCM)	72 × 46, L9	10	Modern
10	LMCELMD4	PMIP1 (AGCM)	48 × 36, L11	15	Modern
11	LMCELMD5	PMIP1 (AGCM)	64 × 50, L11	15	Modern
12	Meteorological Research Institute Model version 2 (MRI2)	PMIP1 (AGCM)	72 × 46, L15	10	Modern
13	U.K. Universities Atmospheric Modeling Global Programme (UGAMP)	PMIP1 (AGCM)	T42L19	20	Modern
14	UIUC11	PMIP1 (AGCM)	72 × 46, L14	10	Modern
15	UKMO	PMIP1 (AGCM)	96 × 73, L19	50	Modern
16	YONU	PMIP1 (AGCM)	72 × 46, L7	10	Modern
17	CCSM3.0	PMIP2 (AOGCM)	T42L18	50	Pre-industrial
18	CSIRO-Mk3L-1.0	PMIP2 (AOGCM)	R21L18	1000	Pre-industrial
19	CSIRO-Mk3L-1.1	PMIP2 (AOGCM)	R21L18	1000	Pre-industrial
20	ECBILTCLIOVECODE	PMIP2 (AOGCM)	T21L3	100	Pre-industrial
21	ECHAME5–MPIOM1	PMIP2 (AOGCM)	T31L20	100	Pre-industrial
22	ECHAM53–MPIOM127-LPJ	PMIP2 (AOGCM)	T31L19	100	Pre-industrial
23	Flexible Global Ocean–Atmosphere–Land System Model gridpoint version 1.0 (FGOALS-1.0g)	PMIP2 (AOGCM)	R42L9	100	Pre-industrial
24	FOAM	PMIP2 (AOGCM)	R15L18	100	Pre-industrial
25	GISS Model E	PMIP2 (AOGCM)	72 × 46, L17	50	Pre-industrial
26	IPSL-CM4-V1-MR	PMIP2 (AOGCM)	96 × 72, L19	100	Pre-industrial
27	Model for Interdisciplinary Research on Climate 3.2 (MIROC3.2)	PMIP2 (AOGCM)	T42L20	100	Pre-industrial
28	MRI-CGCM2.3.4fa	PMIP2 (AOGCM)	T42L30	150	Pre-industrial
29	MRI-CGCM2.3.4nfa	PMIP2 (AOGCM)	T42L30	150	Pre-industrial
30	UBRIS-HadCM3M2	PMIP2 (AOGCM)	96 × 73, L19	100	Pre-industrial
31	ECBILTCLIOVECODE-veg	PMIP2 (AOVGCM)	T21L3	100	Pre-industrial
32	ECHAM53–MPIOM127-LPJ-veg	PMIP2 (AOVGCM)	T31L19	100	Pre-industrial
33	FOAM-veg	PMIP2 (AOVGCM)	R15L18	100	Pre-industrial
34	MRI-CGCM2.3.4fa-veg	PMIP2 (AOVGCM)	T42L30	100	Pre-industrial
35	MRI-CGCM2.3.4nfa-veg	PMIP2 (AOVGCM)	T42L30	100	Pre-industrial
36	UBRIS-HadCM3M2-veg	PMIP2 (AOVGCM)	96 × 73, L19	100	Pre-industrial

has been provided in Table 1. More details relating to the models and experimental designs were given by Joussaume and Taylor (1995) and Braconnot et al. (2007a), and are available online (http://pmip.lsce.ipsl.fr/).

Data used to assess the ability of the models to reproduce the modern temperature climatology over China are taken from the National Centers for Environmental Prediction–National Center for Atmospheric Research (NCEP–NCAR) reanalysis of surface temperature for the period 1979–2000 (Kalnay et al. 1996). Because there are differences in horizontal resolution among the models, all model and reanalysis data are aggregated to a relatively midrange resolution of 96 × 48 (longitude × latitude) using a linear interpolation or extrapolation approach. The ensemble mean of multiple climate models is obtained using the same weights across the models of concern.

b. *Evaluation of the models*

To measure the ability of the models to simulate the baseline temperature climatology over the target region, spatial correlation coefficients (SCCs) and root-mean-square errors (RMSEs) excluding systematic model error of annual and seasonal temperatures between each

TABLE 2. SCCs and RMSEs excluding systematic model error (K) of the annual and seasonal temperature between each baseline (or control) simulation and the observations on the basis of 77 grid points within mainland China. The observational climatology is derived from the NCEP–NCAR reanalysis (Kalnay et al. 1996) for the period 1979–2000 and MME-all denotes the ensemble mean of the 36 models with the same weights.

		Annual		Spring		Summer		Autumn		Winter	
	Model ID	SCC	RMSE	SCC	RMSE	SCC	RMSE	SCC	RMSE	SCC	RMSE
1	CCC2.0	0.88	4.0	0.82	5.5	0.88	3.5	0.89	3.9	0.85	5.8
2	CCM3	0.95	2.5	0.94	2.8	0.91	2.9	0.94	2.8	0.97	2.5
3	CCSR1	0.77	5.4	0.77	6.4	0.49	6.1	0.78	5.3	0.90	5.2
4	CNRM-2	0.91	3.4	0.90	4.2	0.88	3.5	0.90	3.6	0.93	3.9
5	CSIRO	0.93	2.9	0.89	4.6	0.91	3.0	0.94	2.9	0.95	3.4
6	ECHAM3	0.96	2.2	0.94	3.0	0.96	2.0	0.98	1.8	0.96	3.1
7	GEN2	0.95	2.5	0.94	2.9	0.94	2.5	0.94	2.8	0.95	3.3
8	GFDL	0.94	2.8	0.90	4.0	0.92	2.9	0.95	2.6	0.95	3.6
9	GISS-IIP	0.92	3.5	0.92	4.0	0.90	4.7	0.91	3.5	0.95	3.3
10	LMCELMD4	0.95	2.7	0.92	4.0	0.93	2.8	0.95	2.7	0.96	3.6
11	LMCELMD5	0.97	2.5	0.97	3.1	0.91	4.2	0.97	2.5	0.97	2.8
12	MRI2	0.82	4.7	0.78	5.1	0.71	5.0	0.82	4.9	0.88	5.2
13	UGAMP	0.97	2.8	0.95	4.5	0.94	2.7	0.97	2.6	0.97	4.0
14	UIUC11	0.85	4.3	0.82	4.9	0.72	4.9	0.86	4.3	0.92	4.1
15	UKMO	0.99	2.0	0.98	2.2	0.97	2.2	0.99	1.9	0.99	2.4
16	YONU	0.75	5.4	0.58	7.6	0.76	4.6	0.78	5.3	0.86	5.5
17	CCSM3.0	0.94	2.8	0.93	3.1	0.89	3.2	0.94	2.9	0.97	2.7
18	CSIRO-Mk3L-1.0	0.93	2.9	0.93	3.1	0.89	3.2	0.93	3.0	0.96	3.0
19	CSIRO-Mk3L-1.1	0.93	2.9	0.93	3.1	0.89	3.2	0.94	3.0	0.96	3.0
20	ECBILTCLIOVECODE	0.92	3.2	0.91	3.8	0.88	4.7	0.93	3.1	0.95	3.3
21	ECHAME5–MPIOM1	0.89	3.6	0.84	4.5	0.86	3.5	0.94	3.0	0.90	4.7
22	ECHAM53–MPIOM127-LPJ	0.79	4.9	0.73	5.6	0.73	4.8	0.84	4.6	0.85	5.5
23	FGOALS-1.0g	0.98	1.6	0.97	1.8	0.95	2.4	0.98	1.6	0.96	3.0
24	FOAM	0.79	5.0	0.74	5.8	0.74	4.7	0.82	4.9	0.87	5.2
25	GISS Model E	0.95	2.5	0.95	2.7	0.91	3.0	0.95	2.7	0.97	2.4
26	IPSL-CM4-V1-MR	0.96	2.5	0.94	3.3	0.92	3.3	0.97	2.3	0.97	2.8
27	MIROC3.2	0.95	2.8	0.94	3.7	0.93	2.8	0.96	2.5	0.97	3.0
28	MRI-CGCM2.3.4fa	0.95	2.4	0.95	2.6	0.92	2.7	0.96	2.5	0.97	2.7
29	MRI-CGCM2.3.4nfa	0.94	2.7	0.93	3.1	0.93	2.7	0.94	2.8	0.95	3.3
30	UBRIS-HadCM3M2	0.99	1.2	0.98	1.5	0.98	1.6	0.99	1.4	0.98	2.6
31	ECBILTCLIOVECODE-veg	0.92	3.2	0.90	3.8	0.88	4.6	0.93	3.2	0.95	3.4
32	ECHAM53–MPIOM127–LPJ-veg	0.79	4.9	0.74	5.5	0.73	4.8	0.84	4.6	0.85	5.5
33	FOAM-veg	0.79	5.1	0.72	6.1	0.72	4.8	0.82	4.9	0.87	5.1
34	MRI-CGCM2.3.4fa-veg	0.95	2.5	0.94	2.7	0.92	2.7	0.95	2.8	0.96	2.8
35	MRI-CGCM2.3.4nfa-veg	0.92	3.2	0.90	3.6	0.90	3.3	0.92	3.3	0.94	3.7
36	UBRIS-HadCM3M2-veg	0.99	1.4	0.98	1.8	0.98	1.5	0.99	1.4	0.97	3.1
	MME-all	0.96	2.3	0.95	2.7	0.96	2.1	0.96	2.4	0.97	2.5

baseline simulation and the NCEP–NCAR reanalysis data are calculated on the basis of 77 grid points over China, respectively. As given in Table 2, SCCs of annual temperature vary from 0.75 [the Yonsei University Model (YONU] to 0.99 [the Met Office model (UKMO), the Met Office model run at Bristol University–third climate configuration of the Met Office Unified Model (UBRIS-HadCM3M2), and the preindustrialized vegetation version of the UBRIS-HadCM3M2 (UBRIS-HadCM3M2-veg)], and RMSEs of annual temperature vary from 1.2 K (UBRIS-HadCM3M2) to 5.4 K [version 1 of the Center for Climate System Research Model (CCSR1) and YONU]. SCCs (RMSEs) of spring (March–May), summer, autumn (September–November), and winter temperature vary from 0.58 to 0.98 (1.5 to 7.6 K), from 0.49 to 0.98 (1.5 to 6.1 K), from 0.78 to 0.99 (1.4 to 5.3 K), and from 0.85 to 0.99 (2.4 to 5.8 K) across the models. That means the ability of the models to simulate the baseline annual and seasonal temperatures over China varies from model to model. Of importance is that all of the SCCs are positive and statistically significant at the 99% confidence level.

Where the ensemble mean of the 36 models is concerned, Fig. 1 shows clearly that the observational meridional annual temperature gradient in eastern China and a large extent of the low annual temperature over the Qinghai–Tibetan Plateau are well reproduced by the models. Quantitatively, the SCC (RMSE) of annual

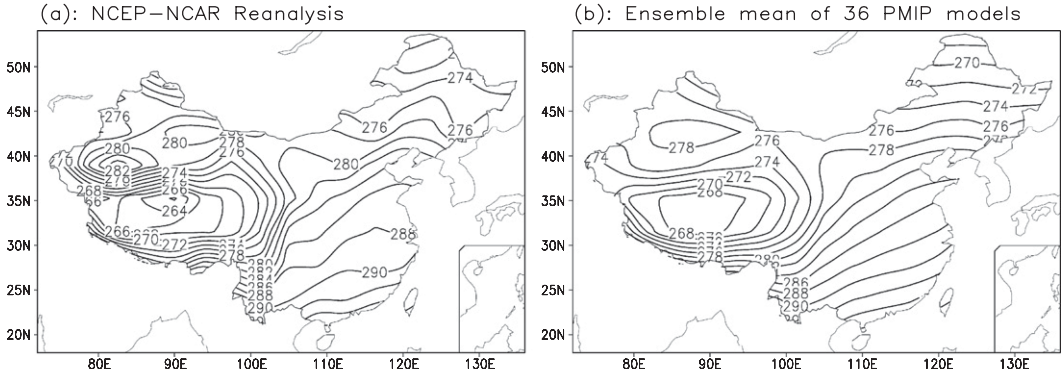

FIG. 1. Annual mean surface temperature (K) from (a) the NCEP–NCAR reanalysis data for the period 1979–2000 (Kalnay et al. 1996) and (b) the 36-model ensemble mean for the baseline period.

temperature is 0.96 (2.3 K), and the SCCs (RMSEs) of seasonal temperature vary from 0.95 to 0.97 (2.1 to 2.7 K). Taken together, all of the models can successfully reproduce the geographical distribution of the baseline annual and seasonal temperatures over China. The 36-model ensemble mean has a higher ability with reference to most, but not all, of the individual models in terms of the values of SCCs and RMSEs. The ensemble mean result of the 36 climate models is therefore emphasized in the following analysis.

3. Mid-Holocene temperature over China from the models

a. Annual temperature change

Thirty-five out of the 36 PMIP models reproduced colder-than-baseline annual temperatures over China during the mid-Holocene (Fig. 2a). The magnitude of the regionally averaged annual temperature change at the national scale was different with the models, ranging from −1.0 K [the 11-layer GCM from the University of Illinois at Urbana–Champaign (UIUC11)] to 0.2 K [L'Institut Pierre-Simon Laplace Coupled Model, version 4 (IPSL-CM4-V1-MR)], with a standard deviation of 0.3 K across the models. Averaged across the whole country and all the models, the annual temperature was reduced by 0.4 K during the mid-Holocene with reference to the baseline climate. On the other hand, the geographical distribution of the mid-Holocene–baseline anomalies in annual temperature varied with the models, particularly at the subregional scale. Where the 36-model ensemble mean is concerned, the annual temperature was slightly elevated by less than 0.1 K over the northern part of northeastern China but reduced by 0–0.8 K over the rest of China during the mid-Holocene (Fig. 3a). Annual temperature cooling was generally greater in the south than in the north over China.

The most important difference between the PMIP1 and PMIP2 models is that ocean dynamics is taken into account in the latter, allowing for an evaluation of the effect of oceans. When viewed in terms of these two model classes, the annual temperature was reduced both in the AGCMs and coupled models (excluding IPSL-CM4-V1-MR), but with a larger magnitude in the former as a whole (Fig. 2a). The regionally averaged annual temperature over China was reduced by 0.6 K from the 16 PMIP1 models, which was greater than the 0.3 K from the 20 PMIP2 models. Meanwhile, the geographical distribution of the changes in the mid-Holocene annual temperature was also different between the model classes (Figs. 3b,c). Over the northern part of northeastern China and northern Xinjiang, the annual temperature was reduced in the PMIP1 models but raised in the PMIP2 models. Over the rest of China, the annual temperature cooling was stronger overall in the PMIP1 models than in the PMIP2 models. According to available SST data from 17 PMIP2 models, Fig. 4a shows that the mid-Holocene annual SSTs differed from the preindustrial period values in the Northern Hemisphere. On one hand, the annual SSTs increased in response to the mid-Holocene orbital forcing in most parts of the northern mid- and high latitudes, with an increase in 16 of the 17 PMIP2 models [excluding the Meteorological Research Institute Coupled General Circulation Model, version 2.3.2a (MRI-CGCM2.3.4nfa)] and an average warming of 0.2 K across all the models within the region of 45°–90°N, 0°–180°. Accordingly, surface temperature increased due to ocean feedback over the high latitudes of Eurasia (Braconnot et al. 2007a). In turn, this favored a surface temperature increase over China, as the warmer air from those areas influenced the regional climate of China, particularly in cold months when northwesterly winds prevailed over the country (e.g., Lau and Li 1984; Gong and Ho 2002). On the other hand, annual SSTs

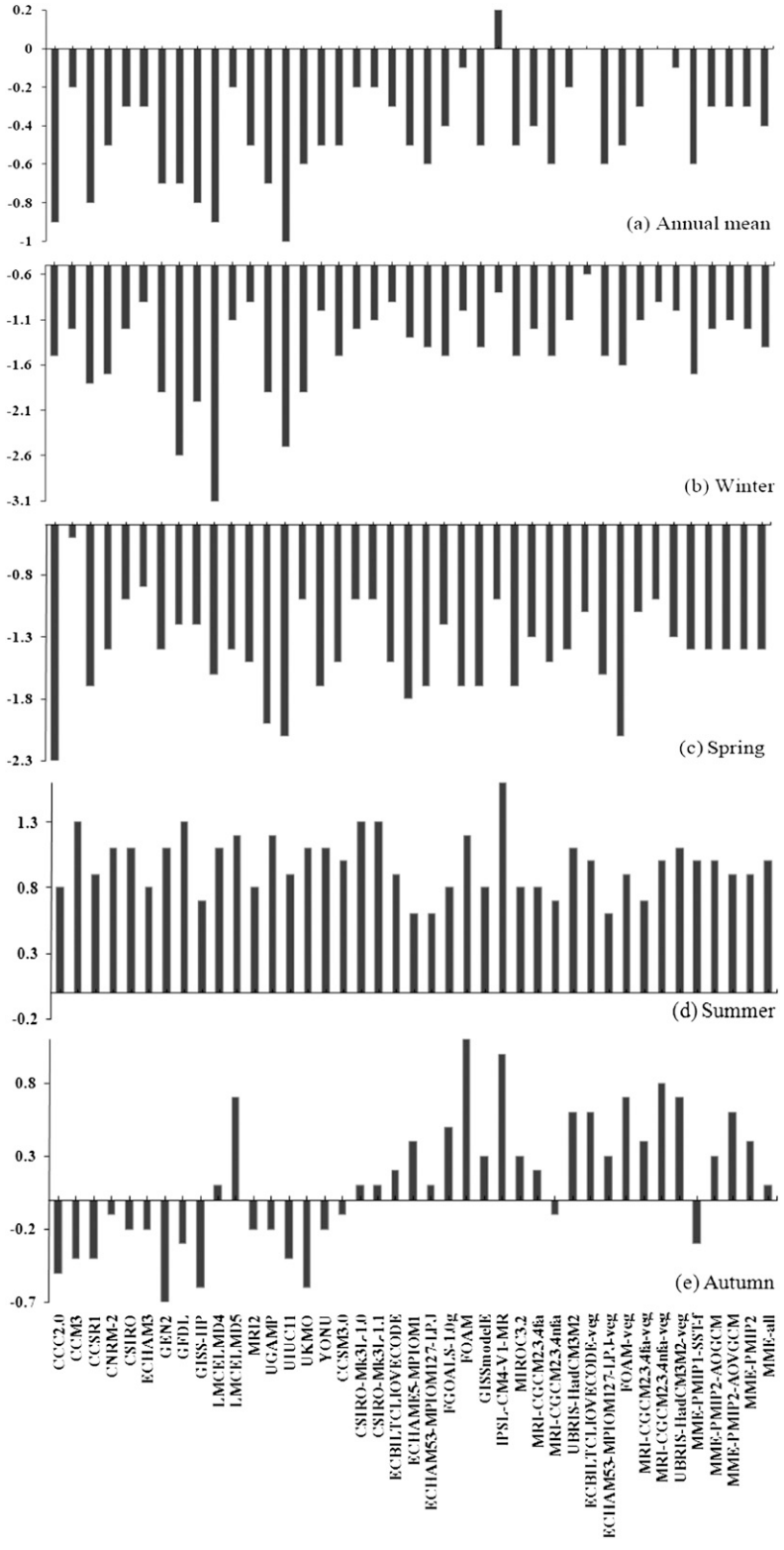

FIG. 2. Mid-Holocene–baseline anomalies of regionally averaged annual and seasonal temperatures (K) over China. Here, MME-PMIP1-SST-f, MME-PMIP2-AOGCM, MME-PMIP2-AOVGCM, MME-PMIP2, and MME-all denote the ensemble mean of the 16 PMIP1 AGCMs, 14 PMIP2 AOGCMs, 6 PMIP2 AOVGCMs, 14 PMIP2 AOGCMs plus 6 PMIP2 AOVGCMs, and 36 PMIP models, respectively.

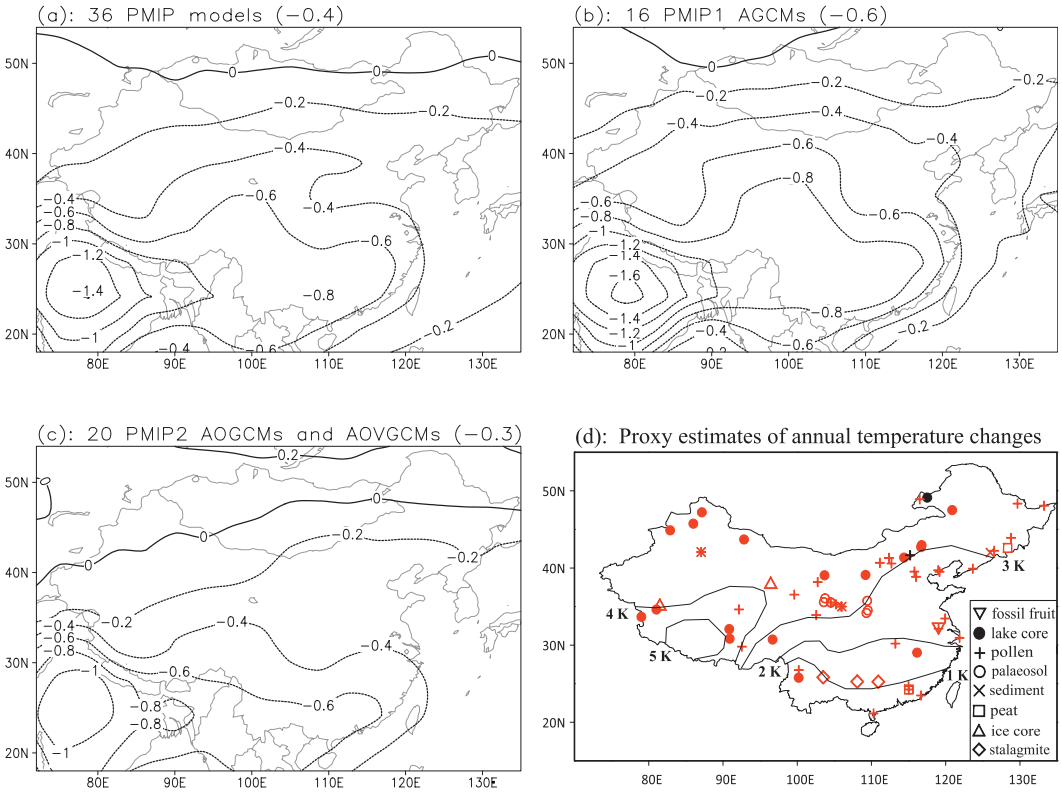

FIG. 3. Mid-Holocene–baseline anomalies of annual temperature (K) for the ensemble mean of the (a) 36 PMIP models, (b) 16 PMIP1 AGCMs, and (c) 14 AOGCMs plus 6 AOVGCMs, with regionally averaged values over China given in parentheses. (d) Proxy estimates of annual temperature changes during the mid-Holocene relative to the present day. Red, black, and blue represent warmer, normal, and colder conditions (see Table 3 for references), respectively, and the contours are from Shi et al. (1993).

decreased overall in the oceans adjacent to the East Asian continent. In the western North Pacific (0°–40°N, 105°E–180°), for example, annual SSTs were generally colder than the baseline values in 13 of the 17 PMIP2 models [excluding Commonwealth Scientific and Industrial Research Organisation Mark version 3.0 (CSIRO-Mk3L-1.0), CSIRO-Mk3L-1.1, the Fast Ocean Atmosphere Model (FOAM), and MRI-CGCM2.3.4nfa-veg], with an average cooling of 0.2 K for the ensemble mean of the 17 models, during the mid-Holocene. This favored a surface temperature decrease over China, because the colder SSTs in that area could lead to larger losses of surface heat in the East Asian region during boreal warm months and smaller gains in surface heat during boreal cold months. In this connection, the response of SSTs to the mid-Holocene forcings needs to be specifically investigated to understand the role of the interactive ocean on the East Asian climate during that period.

Vegetation feedback has been regarded as an important process in the mid-Holocene climate system (Jansen et al. 2007). More specifically, reconstructed paleovegetation was found to be able to cause an overall warming of the annual temperature over China during the mid-Holocene in the earlier experiments using an AGCM (Chen et al. 2002) and two regional climate models (Zheng et al. 2004; Liu et al. 2010a). Also found in those studies were the differences, both in sign and magnitude, of vegetation-induced annual and seasonal temperature changes on a large scale. Such model-dependent results imply a level of uncertainty. Within the PMIP2, 12 simulations were performed by six pairs of climate models, namely, the Climate de Bilt–coupled large-scale ice–ocean model and the Vegetation Continuous Description Model (ECBILTCLIOVECODE), ECHAM53–Max Planck Institute Ocean Model (MPIOM127)–FOAM–Lund Postdam Jena (LPJ), FOAM, MRI-CGCM2.3.4fa, MRI-CGCM2.3.4nfa, UBRIS-HadCM3M2, and their AOVGCM counterparts (Table 1). Importantly, the same AOGCM version was used for both AOGCM and AOVGCM simulations for each pair of the models (T. Fichefet, R. Gladstone, S. Harrison, A. Kitoh, U. Mikolajewicz, and I. Ross 2011, personal communication). These two kinds of parallel simulations provide an opportunity to estimate the role of

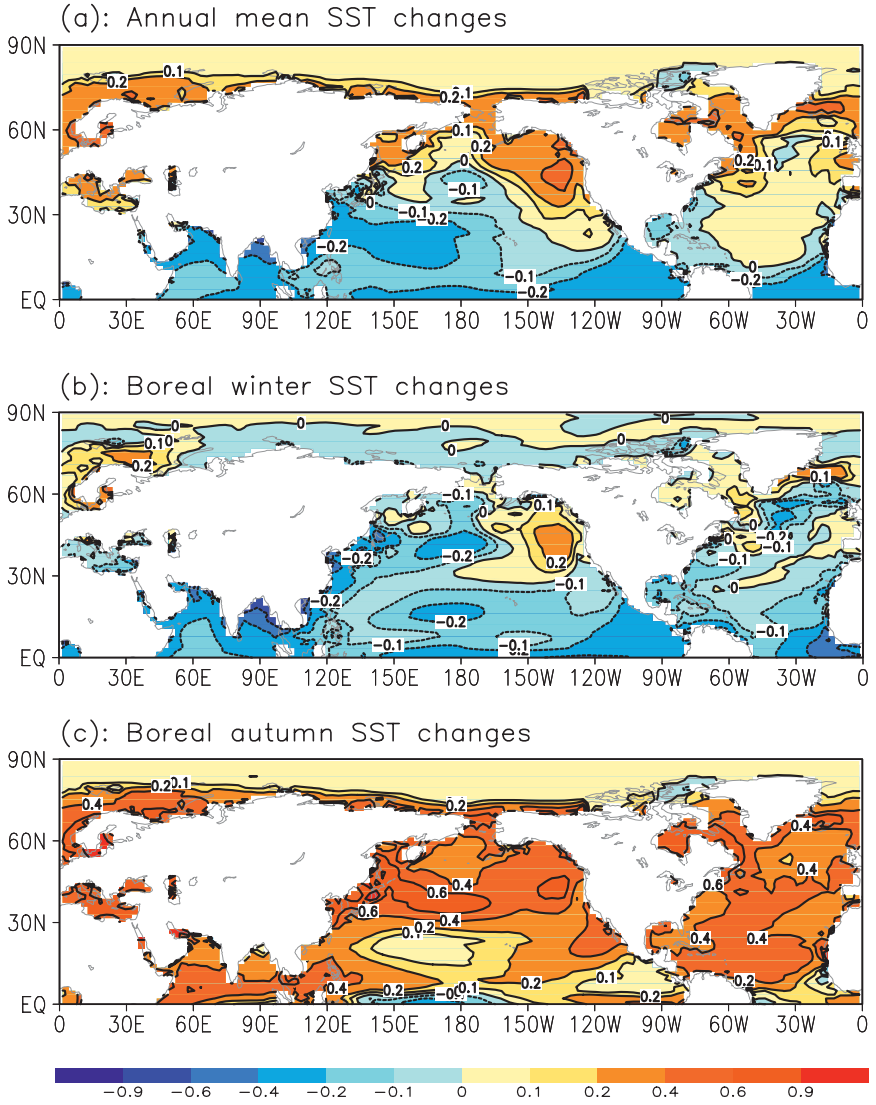

FIG. 4. Mid-Holocene–baseline anomalies of SSTs (K) for the (a) annual mean, (b) winter, and (c) autumn, as derived from 17 of the 20 PMIP2 models (excluding ECHAM5–MPIOM1, ECHAM53–MPIOM127–LPJ, and IPSL-CM4-V1-MR in which SST data are not available).

vegetation within a fully coupled climate model context during the mid-Holocene, as a dynamic global vegetation model component is the main difference between each example.

First, it can be seen in Fig. 5 that interactive vegetation gave rise to additional annual temperature changes during the mid-Holocene. Compared to the values of −0.3 K from ECBILTCLIOVECODE, −0.59 K from ECHAM53–MPIOM127-LPJ, −0.4 K from MRI-CGCM2.3.4fa, −0.6 K from MRI-CGCM2.3.4nfa, and −0.2 K from UBRIS-HadCM3M2 (−0.1 K from FOAM), the corresponding regionally averaged annual temperature changes of −0.02, −0.57, −0.3, −0.04, and −0.1 K (−0.5 K) as derived from their AOVGCM counterparts were weaker (stronger) over China during the mid-Holocene (see Fig. 2a). In this sense, the vegetation effect reduced (amplified) the annual temperature cooling over China in five (one) of the six pairs of the models during that period. Second, Fig. 5 also shows a large spatial variability of vegetation-induced annual temperature changes between each pair of the models. In most parts of China, for example, interactive vegetation led to a strong cooling effect from the FOAM pair, which was opposite to a strong warming effect from the MRI-CGCM2.3.4nfa pair during the mid-Holocene. It is a pity that such results cannot be further investigated in a cause-and-effect manner, as the outputs of vegetation, albedo, leaf area index, and so on, are not yet available in the PMIP

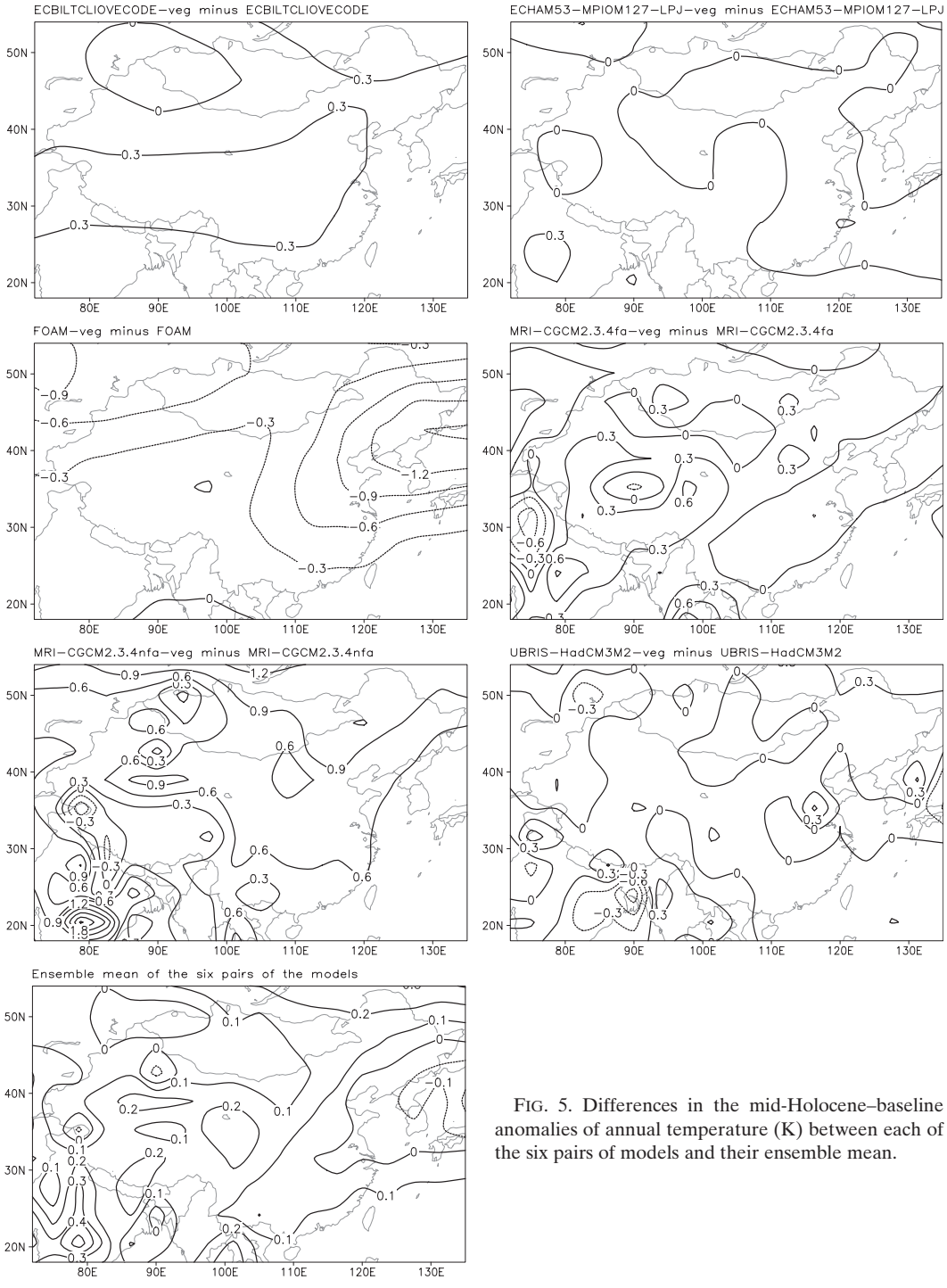

FIG. 5. Differences in the mid-Holocene–baseline anomalies of annual temperature (K) between each of the six pairs of models and their ensemble mean.

database. Third, when averaged over the whole country, the annual temperature change due to the vegetation effect was 0.3 K from the ECBILTCLIOVECODE pair and 0.6 K from the MRI-CGCM2.3.4nfa pair, but −0.4 K from the FOAM pair, respectively. It was around 0–0.1 K from each of the other three pairs of the models. The difference in the mid-Holocene–baseline anomalies in annual temperature between the ensemble mean of the six AOVGCMs and that of the six AOGCMs was less than 0.3 K over China (Fig. 5), with a regionally averaged value of 0.1 K. Taken together, interactive vegetation only gave rise to a weak annual temperature warming,

and it did not appear to be an important component in contributing to the annual temperature change over China during the mid-Holocene.

Note that the modern vegetation was used in the preindustrial experiments of ECBILTCLIOVECODE, FOAM, MRI-CGCM2.3.4fa, and MRI-CGCM2.3.4nfa (T. Fichefet, S. Harrison, A. Kitoh, and I. Ross 2011, personal communication). For each pair of these models, part of the aforementioned vegetation-induced temperature changes during the mid-Holocene is due to the differences between the AOGCM and AOVGCM preindustrial experiments. To investigate vegetation feedback more transparently, the preindustrial vegetation simulated in the AOVGCM preindustrial experiment should be fixed as boundary conditions in the AOGCM experiments so that the AOGCM and AOVGCM mid-Holocene experiments share the similar control experiments (Braconnot et al. 2007b). Averaged over China, the annual temperature difference was 0.04 K between ECHAM53–MPIOM127–LPJ-veg and ECHAM53–MPIOM127–LPJ and –0.001 K between UBRIS-HadCM3M2-veg and the UBRIS-HadCM3M2 preindustrial experiments for which the preindustrial vegetation was used in the AOGCM control experiments (R. Gladstone and U. Mikolajewicz 2011, personal communication). Comparatively, as discussed before, the mid-Holocene annual temperature change was 0.02 K from the ECHAM53–MPIOM127–LPJ pair and 0.1 K from the UBRIS-HadCM3M2 pair. Pure vegetation feedback still has a slight influence on the mid-Holocene annual temperature over the country, which is consistent with the conclusions drawn from all six pairs of the models. Moreover, two recent sets of strict numerical experiments also indicated that the effect of the vegetation feedback on the annual climate over China was quite limited during the mid-Holocene (Dallmeyer et al. 2010; O'ishi and Abe-Ouchi 2011).

b. Seasonal temperature change

According to the work of Berger (1978), the regionally averaged incoming solar radiation at the top of the atmosphere over China was reduced by 11.0 W m^{-2} in winter, 8.2 W m^{-2} in spring, and 3.6 W m^{-2} in autumn, whereas it increased by 21.3 W m^{-2} in summer during the mid-Holocene with respect to the present day. The PMIP experiments indicated that the seasonal temperature change generally followed closely the above insolation change over China during that period. In winter and spring, all 36 models reproduced colder-than-baseline mid-Holocene climates over China (Figs. 2b,c). Winter (spring) temperature cooling varied from 0.6 K in ECBILTCLIOVECODE-veg to 3.1 K in the LMCE model from the Laboratoire des Sciences du Climat et de ÍEnvironnement (LMD, LMCELMD4) [0.5 K in Community Climate Model 3 (CCM3) to 2.3 K in Canadian Centre for Climate Modelling and Analysis (CCCma) Coupled General Circulation Model, version 2.0 (CCC2.0)], with an average of −1.4 K and a standard deviation of 0.5 K (0.4 K) across the 36 models. For the ensemble mean of the 36 models, the mid-Holocene winter (spring) temperature was 0.6–1.9 K (0.9–1.9 K) colder than the baseline climate, with a weaker magnitude over northern China (Figs. 6a,b).

In summer, temperature increased in all of the 36 models during the mid-Holocene (Fig. 2d), ranging from 0.6 K (ECHAM5–MPIOM1, ECHAM53–MPIOM127–LPJ, and ECHAM53–MPIOM127–LPJ-veg) to 1.6 K (IPSL-CM4-V1-MR). Averaged over the country, a warming of 1.0 K, with a standard deviation of 0.2 K, was obtained from the 36 models. Based on the 36-model ensemble mean, the mid-Holocene summer temperature increased by 0–2.3 K over China, except for over the southernmost Tibetan Plateau where weak cooling was presented (Fig. 6c). In addition, warming was more pronounced at high latitudes, which was consistent with the insolation change (Berger 1978).

There was a large discrepancy in the simulated autumn temperature change between the atmospheric and coupled models during the mid-Holocene (Fig. 2e). Fourteen of the 16 PMIP1 AGCMs (excluding LMCELMD4 and LMCELMD5) reproduced colder-than-baseline climates, whereas 18 of the 20 PMIP2 AOGCMs and AOVGCMs [excluding Community Climate System Model, version 3 (CCSM3.0) and MRI-CGCM2.3.4nfa] reproduced warmer-than-baseline climates during the mid-Holocene. The autumn temperature was reduced (increased) by an average of 0.3 K (0.4 K) in terms of the ensemble mean of the 16 PMIP1 (20 PMIP2) models. Averaged across the 36 models, it was increased by 0.1 K, with a standard deviation of 0.5 K. As further seen in Fig. 6d, the mid-Holocene autumn temperature changes were no more than 0.3 K over China, except for over most parts of the Tibetan Plateau where a warming of 0.3–0.7 K occurred.

Compared to the results of the 16 PMIP1 AGCMs, the mid-Holocene seasonal temperature changes as derived from the 20 PMIP2 AOGCMs and AOVGCMs were 0.5 K in winter, 0.03 K in spring, −0.1 K in summer, and 0.7 K in autumn (Fig. 2). In this regard, the interactive ocean led to a warming effect on the winter and autumn temperatures over China during the mid-Holocene, which explained why the above-mentioned annual mean cooling of 0.3 K in the PMIP2 models was weaker than the 0.6-K result found in the PMIP1 models. Similar to the annual mean (Fig. 4a), the mid-Holocene winter SSTs slightly increased overall in the northern high latitudes but decreased in the oceans adjacent to mainland

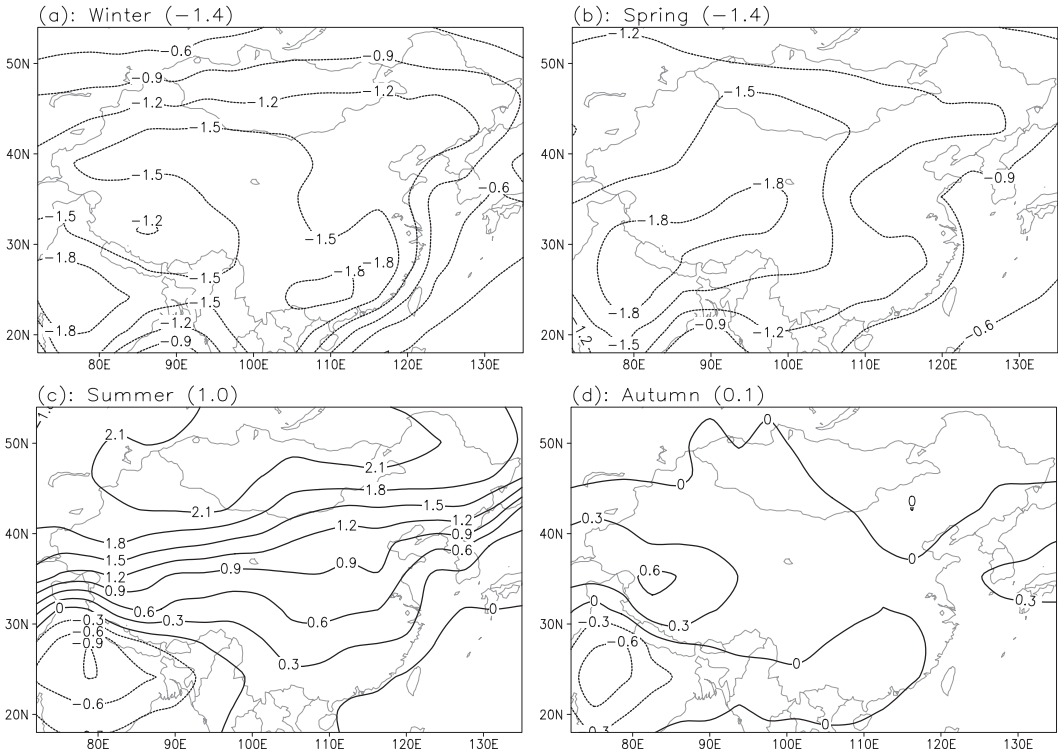

FIG. 6. Mid-Holocene–baseline anomalies of seasonal temperature (K) for the ensemble mean of the 36 models, with regionally averaged values over China given in parentheses.

China, with reference to the baseline values, in terms of the 17-model ensemble mean (Fig. 4b). The former favored a temperature increase, but the latter favored a temperature decrease in winter over China. During the mid-Holocene autumn, all 17 PMIP2 models reproduced warmer-than-baseline SSTs in the Northern Hemisphere, with an average warming of 0.4 K within the region of 0°–90°N, 0°–180° (Fig. 4c). Such SST changes were undoubtedly in favor of autumn warming over China, particularly for those that occurred in the oceans north of Eurasia and adjacent to the East Asian continent.

The vegetation effect also led to additional seasonal temperature changes over China during the mid-Holocene. Averaged across the six pairs of the PMIP2 models and the country, it generally gave rise to a weak warming effect on the seasonal temperature, with the values of 0.1 K in winter, 0.1 K in spring, 0.002 K in summer, and 0.2 K in autumn at the national scale. Seasonal temperature changes due to interactive vegetation were not spatially uniform (Fig. 7). For example, a strong warming (cooling) effect occurred over most parts of the Qinghai–Tibetan Plateau in spring (summer). In addition, there were large differences, both in sign and magnitude, in the simulated vegetation-induced seasonal temperature changes between the pairs of the models. Similar to the annual mean, a strong warming effect was obtained from the ECBILTCLIOVECODE and MRI-CGCM2.3.4nfa pairs, whereas a strong cooling effect was obtained from the FOAM pair. The effect of vegetation was quite small in all of the other three pairs of the models. In summary, interactive vegetation contributed little to seasonal temperature over China during the mid-Holocene. Such results also can be seen in the two recent sets of experiments conducted to examine the pure vegetation feedback during the mid-Holocene (Dallmeyer et al. 2010; O'ishi and Abe-Ouchi 2011).

4. Model–data comparison

A great deal of effort has been made to reconstruct the mid-Holocene climate over China through the use of a variety of proxy data. In this study, two preconditions were set to choose ''reliable'' reconstructions of the mid-Holocene temperature. First, the reconstructions had to be published in peer-reviewed journals, which means that the data quality has been verified by the experts in that field, and second, the reconstructions had to draw a clear conclusion about the mid-Holocene temperature over China. In this manner, the records of pollen, lake

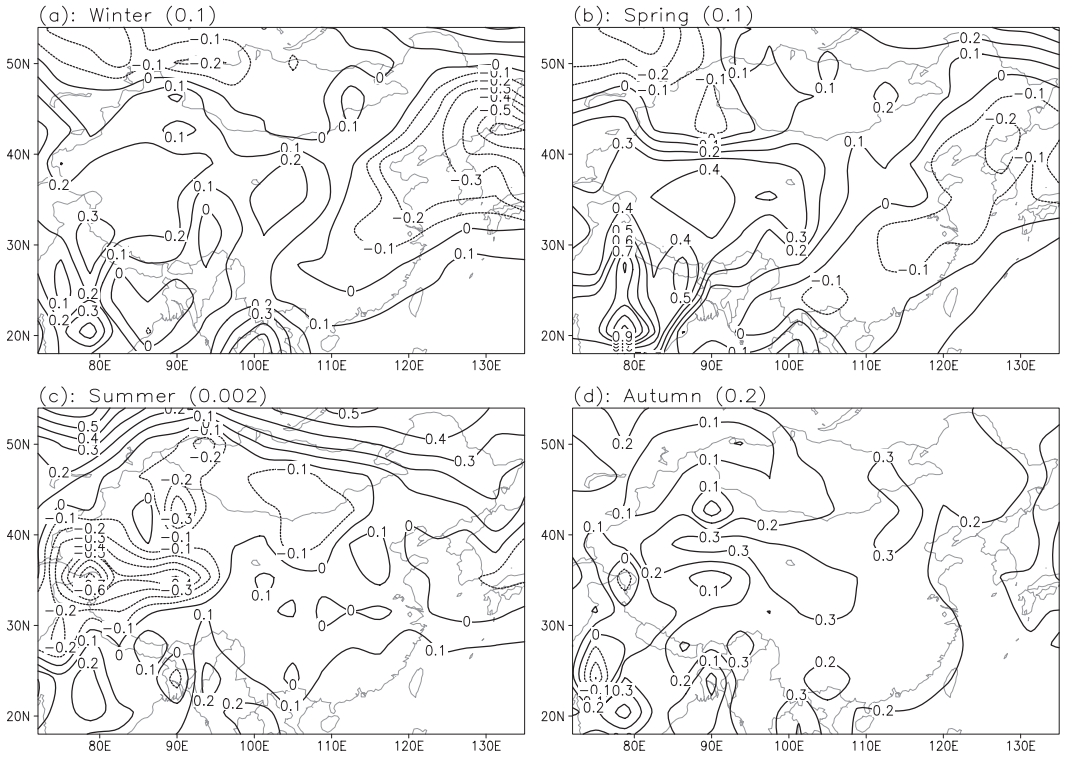

FIG. 7. Vegetation-induced seasonal temperature changes as averaged across the six pairs of the PMIP2 models (K), with regionally averaged values over China given in parentheses.

cores, paleosol, ice cores, peat, sediment, stalagmites, and fossil fruits at 64 sites were finally chosen for the model–data comparison (Table 3). Paleoenvironmental and paleoclimatic evidence from those records indicated that stably warmer climate conditions prevailed over China during the mid-Holocene (Fig. 3d). The annual temperature was elevated by about 1 K in southern China and by about 2 K in the Yangtze River valley in light of the peat profiles and pollen records at Dahu Swamp, the stalagmite records at Dongge Cave, Xiangshui Cave, and Xianrendong Cave, and the pollen assemblage at the Hanjiang Delta, Heqing Basin, and Qingfeng Section. A number of lake cores and pollen records in Inner Mongolia, northern Xinjiang, and Qinghai Lake, together with a few paleosol and peat records, suggested that the annual temperature was about 3 K higher in most parts of northern China. The largest warming of 4–5 K was recorded on the Qinghai–Tibetan Plateau by the lake cores and ice cores. These results are in general consistent with the proxy data before the 1990s, as summarized by Shi et al. (1993), in which the deviation of the annual temperature from the present-day values was roughly estimated to be 1 K in southern China, 2 K in the Yangtze River valley, 3 K in northern and northeastern China, and 4–5 K on the Qinghai–Tibetan Plateau during the mid-Holocene (contours shown in Fig. 3d).

Based on a dataset of 158 pollen samples across China, Yu et al. (1998, 2000) reconstructed the mid-Holocene vegetation of the country. They concluded that the northward shifts of the tropical, broadleaved evergreen/warm mixed, and cool mixed forest zones in eastern China must imply warmer winters than the present because the poleward boundaries of the affected biomes in China today are associated with winter-temperature isotherms that in turn reflect the typical tolerance limits of tropical, subtropical (broadleaved evergreen), and temperate broadleaved deciduous woody plants. The northern boundary of the temperate deciduous forest, which showed the greatest northward shift of all, is also controlled by winter temperatures, occurring where the winter temperatures become cold enough to satisfy the chilling requirements of boreal needle-leaved evergreen trees. Such changes in vegetation and hence generally warmer winters during the mid-Holocene were confirmed by Ni et al. (2010), in which they used 188 pollen samples to reconstruct the paleovegetation over China through a new global classification system of plant functional types and a standard numerical technique for biome assignment. In addition, a few studies suggested

that winter warming was stronger than the annual mean during the mid-Holocene. The existence of Ceratopteris at Baiyangdian and Tancheng during the mid-Holocene, now living in subtropical lakes and swamps, implied that winter temperature was about 6 K warmer than it is today (Xu et al. 1988; Shi et al. 1993). The discovery of nuts from Helicia plants dating back to the mid-Holocene at Baohuashan indicated a 6.3-K warming in January (Kong et al. 1991). Stable forest in the Qinghai Lake area during the mid-Holocene implied a January warming of 8 K (Kong et al. 1990). Pollen records from Bayanchagan, Hidden, Hulun, and Ren Co Lakes also indicated a stronger warming in winter (Tang et al. 2000; Guiot et al. 2008; Jiang et al. 2010; Wen et al. 2010). Using the proxy data before the 1990s, winter warming was estimated to be 70%–100% stronger than that of the annual mean, particularly in eastern China (Shi et al. 1993).

Referring to all of the above, a considerable mismatch existed between the proxy data and the PMIP simulations over China during the mid-Holocene. Contrary to the annual temperature warming as reconstructed by the multiproxy data, 35 of the 36 PMIP models reproduced colder-than-baseline climates, with an average cooling of 0.4 K for all models, over China during the mid-Holocene, particularly in western and northern China where the annual temperature was estimated to be at least 3 K warmer than the present day. Moreover, the winter warming suggested by the proxy data was in stark contrast to the stronger winter cooling, with an average of −1.4 K, as derived from all the models during that period. The annual and winter temperature cooling as derived from the PMIP2 coupled models were weaker overall than those from the PMIP1 AGCMs, and hence they were closer to the proxy data. In this sense, the interactive ocean improved, to a certain extent, the simulation of the mid-Holocene temperature over China. The results of the six AOVGCMs differed little from those of their AOGCM counterparts as a whole. That is, the significant effect of interactive vegetation on annual and seasonal temperatures over China during the mid-Holocene cannot be detected in the present analysis.

Within the protocol of the PMIP experiments, the annual mean incoming solar radiation at the top of the atmosphere was reduced on average by 0.36 W m^{-2} over China during the mid-Holocene (Berger 1978). Additional negative radiative forcing was derived from the changes in atmospheric concentrations of CO_2 in the PMIP1 and CH_4 in the PMIP2 (see section 2). Accordingly, it is no wonder that the PMIP models reproduced colder-than-baseline annual mean climate conditions over the region during that period. Although there are model-dependent uncertainties in the PMIP simulations, of importance is that the intermodel variability of annual and seasonal (excluding autumn) temperature changes, represented by the standard deviation of the model results about their mean, was uniformly smaller than the corresponding ensemble mean result during the mid-Holocene. This implies a robust qualitative consistency on the annual and winter cooling between the models at the national scale. Besides the uncertainties in the simulations, another source that may be partly responsible for the model–data mismatch is the uncertainty in the proxy data. This is especially true for Bayanchagan Lake, where the reconstructed normal climate (Jiang et al. 2006) differed from the warming condition obtained both from the same pollen sample but with different methods (Guiot et al. 2008; Jiang et al. 2010), implying that the method used for climatic reconstruction needs to be carefully evaluated, and from the lake cores and pollen records at surrounding sites (Fig. 3d). At Hulun Lake, the normal temperature derived from the lake cores (Wen et al. 2010) was also different from the warming derived from the pollen records (Yang et al. 1995; Fig. 3d). However, given that the mid-Holocene warmer climates were consistently inferred from all of the other 62 sites (Table 3 and Fig. 3d) through multiple proxies and approaches and from proxy data before the 1990s (Shi et al. 1993), and that the mid-Holocene warmer winter climates were consistently suggested by 158 (Yu et al. 2000) and 188 pollen samples (Ni et al. 2010), proxy data at a few sites (Table 3), and proxy data before the 1990s (Shi et al. 1993) across China, they should be reliable, at least in a qualitative manner. Collectively, the aforementioned model–data mismatch in annual and winter temperatures over China during the mid-Holocene appears to be robust.

5. Conclusions

Responding faithfully to the imposed negative radiative forcing derived from changes in the earth's orbital parameters and atmospheric concentrations of CO_2 or CH_4 during the mid-Holocene, 35 out of the 36 PMIP models reproduced colder-than-baseline annual temperature over China, with a larger magnitude overall in atmospheric models than in coupled models. In all the models, seasonal temperature was significantly reduced in winter and spring, whereas it was significantly elevated in summer. In autumn, temperature was generally reduced in atmospheric models but elevated in coupled models, which was related to warmer-than-baseline SSTs in the oceans north of Eurasia and in the western North Pacific as computed by coupled models. Based on the multiproxy data at 64 sites (Table 3 and Fig. 3d),

TABLE 3. Proxy data providing estimates of annual temperature changes ΔT between the mid-Holocene and the present day over China.

Site	Proxy data	Lat (°N)	Lon (°E)	Elevation (m ASL)	Interval (ka)	ΔT	Reference
Aibi Lake	Lake core	44.88	82.88	194	10.2	Warmer	Wu et al. (1996)
Angulinao Lake	Lake core	41.35	114.39	1310	8.4	Warmer	Zhai et al. (2000)
Baahar Nuur Lake	Lake core	39.10	109.20	1450	13.9	Warmer	Feng et al. (2005)
Baimapo	Palaeosol	34.17	109.32	650	20.6	Warmer	Zhou et al. (1994)
Baiyangdian Lake	Pollen	38.85	116.00	7	11.0	2–4 K warmer	Xu et al. (1988)
Bangong Co Lake	Lake core	33.67	79.00	4241	10.0	Warmer	Gasse et al. (1996)
Baohuashan	Fossil fruit, pollen	32.13	119.03	5	5.1	3.5 K warmer, 6.3 K warmer in January	Kong et al. (1991)
Barkol Lake	Lake core	43.70	92.83	1580	9.4	Warmer	Xue and Zhong (2008)
Baxie	Palaeosol	35.58	103.57	2000	12.3	Warmer	Zhou et al. (1994)
Bayanchagan Lake	Pollen	41.65	115.21	1355	12.5	Normal	Jiang et al. (2006)
Bayanchagan Lake	Pollen	41.65	115.21	1355	12.5	Warmer, stronger warming in January	Guiot et al. (2008), Jiang et al. (2010)
Beizhuangcun	Palaeosol	34.50	109.50	950	26.1	Warmer	Zhou et al. (1994)
Bosten Lake	Sediment, pollen	42.08	87.05	1500	12.0	Warmer	Zhong and Shu (2001)
Changbaishan	Peat	40.67–44.50	125.33–131.33	500–900	10.0	Warmer	Zhao et al. (2002)
Chasuqi	Pollen	40.67	111.13	1000	9.1	Warmer	Wang and Sun (1997)
Dadiwan	Pollen	35.01	105.91	1400	11.2	Warmer	An et al. (2003)
Dagushan	Pollen	39.92	123.66	5	8.0–2.5	3–5 K warmer	Laboratory of Quaternary Palynology and Laboratory of Radiocarbon, Kweiyang Institute of Geochemistry, Academia Sinica (1978)
Dahu	Peat, pollen	24.25	115.03	250	18.0	Around 1–2 K warmer	Zhou et al. (2004)
Dahu	Pollen	24.68	115.00	255	18.3	Warmer	Xiao et al. (2007)
Daihai Lake	Pollen	40.58	112.69	1221	12.0	Warmer, around 3 K warmer in July	Xu et al. (2003)
Daziying	Pollen	39.70	118.99	5	9.8	Warmer	Li and Liang (1985)
Diaojiao Lake	Pollen	41.30	112.35	1800	10.1	Warmer	Song et al. (1996)
Diaojiao Lake	Pollen	41.30	112.35	1800	10.1	3–6 K warmer	Shi and Song (2003)
Dingxi	Palaeosol	35.52	104.54	1950	8.9	Warmer	Feng et al. (2005)
Dongganchi	Pollen	39.53	115.78	49	15.8	Warmer	Zhang and Kong (1999)
Dongge Cave	Stalagmite	25.28	108.08	680	15.4	Warmer	Zhang et al. (2004)
Donghai	Pollen	30.95	121.87	5	8.0	Around 2 K warmer	Zhang (2006)
Dunde	Ice core	38.10	96.42	5325	10.6	Warmer	Wei and Lin (1994)
Erhai Lake	Lake core	25.78	100.19	1974	8.1	Warmer	Zhang et al. (2000a)
Gonong Co	Pollen	34.63	92.15	4670	19.2	Warmer	Li et al. (1995)
Guliya	Ice core	35.28	81.48	6200	125.0	1.5 K warmer	Yao et al. (1997)
Gushantun	Sediment	42.00	126.00	500	13.5	Warmer	Wang and Liu (2001)

TABLE 3. (*Continued*)

Site	Proxy data	Lat (°N)	Lon (°E)	Elevation (m ASL)	Interval (ka)	ΔT	Reference
Ha'ni	Pollen	42.23	126.52	900	13.1–4.5	Warmer	Yu et al. (2008)
Hanjiang Delta	Pollen	23.48	116.68	8	10.0	1–2 K warmer	Zheng (1990)
Haoluku Lake	Lake core	42.96	116.76	1295	10.2	Warmer	Wang et al. (2001)
Heqing Basin	Pollen	26.77	100.21	2200	30.0	Warmer	Jiang et al. (1998)
Hidden Lake	Pollen	29.81	92.54	4980	14.0	2–3 K warmer in January and July	Tang et al. (2000)
Hongshui River	Pollen	38.18	102.76	1460	8.5–3.0	Warmer	Zhang et al. (2000b)
Huguangyan Maar Lake	Pollen	21.15	110.28	23	13.0	Warmer	Wang et al. (2007)
Hulu River	Sediment, pollen	35.00	106.00	1540	8.0–3.0	Warmer	Mo et al. (1996)
Hulun Lake	Pollen	48.90	116.50	544	19.9	Around 3 K warmer	Yang et al. (1995)
Hulun Lake	Lake core	49.13	117.51	545	11.0	Normal, 3 K warmer in January	Wen et al. (2010)
Jingbo Lake	Pollen	43.90	128.80	350	9.6	Warmer	Li et al. (2011)
Jiuzhoutai	Palaeosol	36.07	103.75	2067	10.0	Warmer	Chen et al. (1991)
Liuzhouwan	Lake core	42.71	116.68	1365	13.4	Warmer	Wang et al. (2001)
Longzhong Basin	Pollen	35.00–35.55	104.52–105.91	1400–1889	12.2	Warmer	Tang and An (2007)
Manas Lake	Lake core	45.75	86.00	251	37.0	Warmer	Rhodes et al. (1996)
Maohebei	Pollen	39.50	119.17	50	10.3	Warmer	Li and Liang (1985)
Mianyang	Pollen	30.20	113.22	24	10.0	Warmer	Yang et al. (1998)
Moon Lake	Lake core	47.51	120.87	1190	21.0	Warmer	Liu et al. (2010b)
Nam Co Lake	Lake core	30.84	90.90	4718	8.4	Warmer	Zhu et al. (2007)
Poyang Lake	Lake core	29.03	116.14	8	7.9	Warmer	Ma et al. (2004)
Qingfeng	Pollen	33.45	119.92	2	10.0	Around 1 K warmer	Zhao et al. (1994)
Qinghai Lake	Pollen	36.55	99.60	3196	11.0	Warmer, 8–11 K warmer in January, 2 K warmer in July	Kong et al. (1990)
Qingtu Lake	Lake core	39.05	103.67	1309	9.0–3.0	Warmer	Long et al. (2007)
Ren Co Lake	Lake core	30.73	96.68	4450	18.0	2–3 K warmer in January and July	Tang et al. (2000)
Renjiahutong	Palaeosol	35.75	109.42	1100	13.0	Warmer	Zhou et al. (1994)
Sujiawan	Palaeosol, pollen	35.54	104.52	1700	8.9	Warmer	An et al. (2003)
Sumxi Co Lake	Lake core	34.62	81.03	5058	13.0	Warmer	Gasse et al. (1991)
Tanghongling	Pollen	48.35	129.67	465	9.0	1–2 K warmer	Yang and Wang (2002)
Tongjiang	Pollen	48.08	133.25	60	8.0	2–3 K warmer	Yang and Wang (2003)
Ulungur Lake	Lake core	47.22	87.15	478	9.9	Warmer	Jiang et al. (2007)
Xiangshui Cave	Stalagmite	25.25	110.92	400	6.0	Warmer	Zhang et al. (2003)
Xianrendong Cave	Stalagmite	25.83	103.50	1810	8.0	Warmer	Zhang et al. (2009)
Zigê Tangco	Lake core	32.08	90.84	4560	10.5	Warmer	Wu et al. (2007)
Zoige	Pollen	33.90	102.55	3396	20.0	Warmer	Liu et al. (1995)

a number of proxy data before the 1990s (Shi et al. 1993), and 158 and 188 pollen samples (Yu et al. 2000; Ni et al. 2010) across China, the mid-Holocene annual temperature of the country was estimated to be around 1–5 K warmer than the present-day values, while winter warming was also warmer than that of today. Taken together, the colder annual and winter climates from the PMIP models are the opposite of those from the multiproxy records.

Interactive ocean gave rise to an additional warming of 0.5 K in winter and 0.7 K in autumn over China, and hence the annual and winter temperatures of coupled models were in better agreement with proxy data than those of atmospheric models during the mid-Holocene. Averaged across the country and the six pairs of PMIP2 models, interactive vegetation was found to have little effect on the mid-Holocene annual and seasonal temperatures. The same conclusion was drawn from the experiments of the ECHAM53–MPIOM127-LPJ and UBRIS-HadCM3M2 pairs for which the preindustrial vegetation was used in the AOGCM control experiments. On the other hand, the spread of vegetation-induced temperature changes between each of the six pairs of the models implies a level of uncertainty in the mid-Holocene vegetation effect in the East Asian monsoon areas, which needs to be specifically investigated within the context of cause and effect. In this respect, the AOGCM and AOVGCM experiments of the mid-Holocene climate should share the same or similar control experiments, as suggested by Braconnot et al. (2007a,b), Dallmeyer et al. (2010), and O'ishi and Abe-Ouchi (2011). In addition, the extent to which the simulated vegetation from AOVGCMs is compatible with the reconstruction (e.g., Yu et al. 2000; Ni et al. 2010) during the mid-Holocene should be evaluated.

Note that the present model–data mismatch in annual and winter temperatures over China during the mid-Holocene was derived from a variety of proxy data and the experiments of 36 climate models. At the moment it is unclear whether the inconsistency arises from the models, from the proxy data, or from both sides. If the interpretations of those proxy data are correct, this raises an important question as to the dynamic mechanism underlying the mid-Holocene East Asian climate change and also poses a challenge for the forthcoming PMIP simulations of the regional climate over China for that period. Examining how, and to what extent, the new generation of climate models and/or earth system models participating in the third stage of the PMIP respond to the mid-Holocene forcing over the country is of particular interest. Whether the missing biogeochemical processes in the previous models affect the mid-Holocene East Asian climate should be examined using earth system models with carbon and nitrogen dynamics. The impact of model biases in simulating the modern climate on model results for the mid-Holocene also should be given special attention at the regional scale (e.g., Braconnot et al. 2002; Ohgaito and Abe-Ouchi 2009). On the other hand, as discussed before, the models seem to do what is asked of them in terms of negative radiative forcing over the country. Is it possible that the paleoarchives are not actually able to record the information that is equivalent to temperature in the models? Interestingly, the mid-Holocene temperature was shown to be colder in part of China in the works of Guiot et al. (2008) and Bartlein et al. (2011) using the modern analog, regression, and model-inversion techniques, in which the general challenge is that there is not a strong direct functional or mechanistic relationship between pollen spectra and climatic variables because pollen production is affected by the interaction of a large number of nonlinear processes (Ohlwein and Wahl 2012). Although there are inconsistencies between their results, for example warmer in the former versus colder in the latter over northeastern China, they at least indicate the uncertainty of the mid-Holocene warming from single-site reconstructions over China. Additionally, it should be kept in mind that the spatial coverage of the proxy data used for the present model–data comparison is still sparse. Collectively, more reconstruction work using multiple proxies and methods is required to narrow the uncertainty of proxy data and then test the model results, which is important to our understanding the mid-Holocene climate in the East Asian monsoon area. In that field, as discussed in the model–data comparison section, the method used for climatic reconstruction should be carefully assessed and validated.

Finally, it is noted that the PMIP2 CCSM3.0 simulations have been used to discuss the East Asian winter monsoon during the mid-Holocene (Zhou and Zhao 2009). The present analysis adds an important caveat to these kinds of studies, since an average cooling of 1.5 K as simulated by this model disagreed qualitatively with the proxy data over China during the mid-Holocene winter.

Acknowledgments. We sincerely thank the three anonymous reviewers and Dr. Anthony J. Broccoli for their helpful comments and suggestions on the earlier versions of the manuscript; Thierry Fichefet, Rupert Gladstone, Sandy Harrison, Akio Kitoh, Uwe Mikolajewicz, and Ian Ross for information on the PMIP2 AOVGCMs and their AOGCM counterparts; and Fahu Chen, Zhaodong Feng, Wenying Jiang, Bingcheng Li, Hongya Wang, Jüle Xiao, and Xuefeng Yu for information on proxy data. Also, we acknowledge the

international modeling groups for providing their data for analysis, and the Laboratoire des Sciences du Climat et de l'Environnement (LSCE) for collecting and archiving the model data. This research was supported by the Chinese National Basic Research Program (2009CB421407), the Strategic Priority Research Program (XDA05120703) and the Knowledge Innovation Program (KZCX2-EW-QN202) of the Chinese Academy of Sciences, and the National Natural Science Foundation of China (40975050 and 41175072). The PMIP2/MOTIF Data Archive is supported by CEA, CNRS, the EU project MOTIF (EVK2-CT-2002-00153), and the Programme National d'Etude de la Dynamique du Climat (PNEDC). The analyses were performed using version 9 August 2010 of the database. More information is available online (http://pmip2.lsce.ipsl.fr/ and http://motif.lsce.ipsl.fr/).

REFERENCES

An, C., Z. Feng, and L. Tang, 2003: Evidence of a humid mid-Holocene in the western part of Chinese Loess Plateau. *Chin. Sci. Bull.,* **48,** 2472–2479.

Bartlein, P. J., and Coauthors, 2011: Pollen-based continental climate reconstructions at 6 and 21 ka: A global synthesis. *Climate Dyn.,* **37,** 775–802.

Berger, A., 1978: Long-term variations of daily insolation and Quaternary climatic changes. *J. Atmos. Sci.,* **35,** 2362–2367.

Bonfils, C., N. de Noblet-Ducoudré, J. Guiot, and P. Bartlein, 2004: Some mechanisms of mid-Holocene climate change in Europe, inferred from comparing PMIP models to data. *Climate Dyn.,* **23,** 79–98.

Braconnot, P., M.-F. Loutre, B. Dong, S. Joussaume, P. Valdes, and PMIP Participating Groups, 2002: How the simulated change in monsoon at 6 ka BP is related to the simulation of the modern climate: Results from the Paleoclimate Modeling Intercomparison Project. *Climate Dyn.,* **19,** 107–121.

——, and Coauthors, 2007a: Results of PMIP2 coupled simulations of the mid-Holocene and Last Glacial Maximum—Part 1: Experiments and large-scale features. *Climate Past,* **3,** 261–277.

——, and Coauthors, 2007b: Results of PMIP2 coupled simulations of the mid-Holocene and Last Glacial Maximum—Part 2: Feedbacks with emphasis on the location of the ITCZ and mid- and high latitudes heat budget. *Climate Past,* **3,** 279–296.

Chen, F. H., J. J. Li, and W. X. Zhang, 1991: Loess stratigraphy of the Lanzhou profile and its comparison with deep-sea sediment and ice core record. *GeoJournal,* **24,** 201–209.

Chen, X., G. Yu, and J. Liu, 2002: Mid-Holocene climate simulation and discussion on the mechanism of temperature changes in eastern Asia (in Chinese). *Sci. China,* **32D,** 335–345.

Dallmeyer, A., M. Claussen, and J. Otto, 2010: Contribution of oceanic and vegetation feedbacks to Holocene climate change in monsoonal Asia. *Climate Past,* **6,** 195–218.

Feng, Z. D., and Coauthors, 2005: Lacustrine and eolian records of Holocene climate changes in the Mongolian Plateau: Preliminary results. *Quat. Int.,* **136,** 25–32.

Gasse, F., and Coauthors, 1991: A 13,000-year climate record from western Tibet. *Nature,* **353,** 742–745.

——, J. C. Fontes, E. Van Campo, and K. Wei, 1996: Holocene environmental changes in Bangong Co basin (western Tibet). Part 4: Discussion and conclusions. *Palaeogeogr. Palaeoclimatol. Palaeoecol.,* **120,** 79–92.

Gong, D.-Y., and C.-H. Ho, 2002: The Siberian high and climate change over middle to high latitude Asia. *Theor. Appl. Climatol.,* **72,** 1–9.

Guiot, J., J. J. Boreux, P. Braconnot, F. Torre, and PMIP Participants, 1999: Data–model comparison using fuzzy logic in paleoclimatology. *Climate Dyn.,* **15,** 569–581.

——, H. B. Wu, W. Y. Jiang, and Y. L. Luo, 2008: East Asian monsoon and paleoclimatic data analysis: A vegetation point of view. *Climate Past,* **4,** 137–145.

Hoar, M. R., J. P. Palutikof, and M. C. Thorne, 2004: Model intercomparison for the present day, the mid-Holocene, and the Last Glacial Maximum over western Europe. *J. Geophys. Res.,* **109,** D08104, doi:10.1029/2003JD004161.

Jansen, E., and Coauthors, 2007: Palaeoclimate. *Climate Change 2007: The Physical Science Basis,* S. Solomon et al., Eds., Cambridge University Press, 434–497.

Jiang, Q. F., J. Shen, X. Q. Liu, and E. L. Zhang, 2007: Holocene climate reconstruction of Ulungur Lake (Xinjiang, China) inferred from ostracod species assemblages and stable isotopes (in Chinese). *Quat. Sci.,* **27,** 382–391.

Jiang, W., Z. Guo, X. Sun, H. Wu, G. Chu, B. Yuan, C. Hatté, and J. Guiot, 2006: Reconstruction of climate and vegetation changes of Lake Bayanchagan (Inner Mongolia): Holocene variability of the East Asian monsoon. *Quat. Res.,* **65,** 411–420.

——, J. Guiot, G. Chu, H. Wu, B. Yuan, C. Hatté, and Z. Guo, 2010: An improved methodology of the modern analogues technique for palaeoclimate reconstruction in arid and semi-arid regions. *Boreas,* **39,** 145–153.

Jiang, X. Z., S. M. Wang, and X. D. Yang, 1998: Paleoclimatic and environmental changes over the last 30000 years in Heqing Basin, Yunnan Province (in Chinese). *J. Lake Sci.,* **10,** 10–16.

Joussaume, S., and K. E. Taylor, 1995: Status of the Paleoclimate Modeling Intercomparison Project (PMIP). *Proceedings of the First International AMIP Scientific Conference,* W. L. Gates, Ed., WCRP-92, WMO/TD-732, 425–430.

Kalnay, E., and Coauthors, 1996: The NCEP/NCAR 40-Year Reanalysis Project. *Bull. Amer. Meteor. Soc.,* **77,** 437–471.

Kong, Z. C., N. Q. Du, F. S. Shan, G. B. Tong, S. J. Luo, and S. X. Fan, 1990: Vegetational and climatic changes in the last 11,000 years in Qinghai Lake—Numerical analysis based on palynology in core QH85-14C (in Chinese). *Mar. Geol. Quat. Geol.,* **10,** 79–90.

——, ——, Y. J. Zhang, F. B. Wang, Y. L. Liang, and X. C. Wang, 1991: Discovery of Helicia fossil florule and sporo-pollen assemblage of Baohuashan in Jurong County and its climatic and botanic significance (in Chinese). *Quat. Sci.,* **11,** 326–335.

Laboratory of Quaternary Palynology and Laboratory of Radiocarbon, Kweiyang Institute of Geochemistry, Academia Sinica, 1978: Development of natural environment in the southern part of Liaoning Province during the last 10,000 years. *Sci. Sin.,* **21A,** 516–532.

Lau, K.-M., and M.-T. Li, 1984: The monsoon of East Asia and its global associations—A survey. *Bull. Amer. Meteor. Soc.,* **65,** 114–125.

Li, B. Y., Y. F. Li, Z. C. Kong, F. S. Shan, L. P. Zhu, and S. K. Li, 1995: 20,000 years environmental changes of the Gonong Co in Hoh Xil of Qinghai. *Chin. Sci. Bull.,* **40,** 1055–1056.

Li, C. H., Y. H. Wu, and X. H. Hou, 2011: Holocene vegetation and climate in northeast China revealed from Jingbo Lake sediment. *Quat. Int.,* **229,** 67–73.

Li, W. Y., and Y. L. Liang, 1985: Vegetation and environment of the Hypsithermal Interval of Holocene in eastern Hebei Plain (in Chinese). *Acta Bot. Sin.,* **27,** 640–651.

Liu, G. X., Y. P. Shen, R. Wang, and S. M. Wang, 1995: The vegetation and climatic changes in Zoige during the last 20000 years determined by pollen records (in Chinese). *J. Glaciol. Geocryol.,* **17,** 132–137.

Liu, Q., Q. Li, L. Wang, and G. Q. Chu, 2010b: Stable carbon isotope record of bulk organic matter from a sediment core at Moon Lake in the middle part of the Daxing'an Mountain range, northeast China during the last 21 ka (in Chinese). *Quat. Sci.,* **30,** 1069–1077.

Liu, Y., J. He, W. Li, L. Chen, W. Li, and B. Zhang, 2010a: MM5 simulations of the China regional climate during the mid-Holocene. *Acta Meteor. Sin.,* **24,** 468–483.

Long, H., H. B. Tan, N. A. Wang, L. C. Tan, and Y. Li, 2007: Mid-Holocene climate variations recorded by palaeolake in marginal area of East Asian monsoon: A multi-proxy study. *Chin. Geogr. Sci.,* **17,** 325–332.

Ma, Z. X., J. H. Huang, Y. Wei, J. H. Li, and C. Y. Hu, 2004: Organic carbon isotope records of the Poyang Lake sediments and their implications for the paleoclimate during the last 8 ka (in Chinese). *Geochimica,* **33,** 279–285.

Masson, V., R. Cheddadi, P. Braconnot, S. Joussaume, D. Texier, and PMIP Participants, 1999: Mid-Holocene climate in Europe: What can we infer from PMIP model–data comparisons? *Climate Dyn.,* **15,** 163–182.

Masson-Delmotte, V., and Coauthors, 2006: Past and future polar amplification of climate change: Climate model intercomparisons and ice-core constraints. *Climate Dyn.,* **26,** 513–529.

Mo, D. W., F. Li, S. C. Li, and Z. C. Kong, 1996: A preliminary study of the paleoenvironment of the middle Holocene in the Hulu River area in Gansu Province and its effects on human activity (in Chinese). *Acta Geogr. Sin.,* **51,** 59–69.

Ni, J., G. Yu, S. P. Harrison, and I. C. Prentice, 2010: Palaeovegetation in China during the late Quaternary: Biome reconstructions based on a global scheme of plant functional types. *Palaeogeogr. Palaeoclimatol. Palaeoecol.,* **289,** 44–61.

Ohgaito, R., and A. Abe-Ouchi, 2009: The effect of sea surface temperature bias in the PMIP2 AOGCMs on mid-Holocene Asian monsoon enhancement. *Climate Dyn.,* **33,** 975–983.

Ohlwein, C., and E. R. Wahl, 2012: Review of probabilistic pollen-climate transfer methods. *Quat. Sci. Rev.,* **31,** 17–29.

O'ishi, R., and A. Abe-Ouchi, 2011: Polar amplification in the mid-Holocene derived from dynamical vegetation change with a GCM. *Geophys. Res. Lett.,* **38,** L14702, doi:10.1029/2011GL048001.

Peyron, O., D. Jolly, P. Braconnot, R. Bonnefille, J. Guiot, D. Wirrmann, and F. Chalié, 2006: Quantitative reconstructions of annual rainfall in Africa 6000 years ago: Model–data comparison. *J. Geophys. Res.,* **111,** D24110, doi:10.1029/2006JD007396.

Rhodes, T. E., and Coauthors, 1996: A late Pleistocene–Holocene lacustrine record from Lake Manas, Zunggar (northern Xinjiang, western China). *Palaeogeogr. Palaeoclimatol. Palaeoecol.,* **120,** 105–121.

Shi, P. J., and C. Q. Song, 2003: Palynological records of environmental changes in the middle part of Inner Mongolia, China. *Chin. Sci. Bull.,* **48,** 1433–1438.

Shi, Y., and Coauthors, 1993: Mid-Holocene climates and environments in China. *Global Planet. Change,* **7,** 219–233.

Song, C. Q., B. Y. Wang, and X. J. Sun, 1996: Implication of paleovegetational changes in Diaojiao Lake, Inner Mongolia (in Chinese). *Acta Bot. Sin.,* **38,** 568–575.

Tang, L. Y., and C. B. An, 2007: Pollen records of Holocene vegetation and climate changes in the Longzhong Basin of the Chinese Loess Plateau. *Prog. Nat. Sci.,* **17,** 1445–1456.

——, C. M. Shen, K. Liu, and J. T. Overpeck, 2000: Changes in South Asian monsoon: New high-resolution paleoclimatic records from Tibet, China. *Chin. Sci. Bull.,* **45,** 87–91.

Wang, B. Y., and X. J. Sun, 1997: Primary study on the Holocene environment changes in Chasuqi peat, Inner Mongolia (in Chinese). *Chin. Sci. Bull.,* **42,** 514–518.

Wang, H. J., 1999: Role of vegetation and soil in the Holocene megathermal climate over China. *J. Geophys. Res.,* **104** (D8), 9361–9367.

——, 2000: The seasonal climate and low frequency oscillation in the simulated mid-Holocene megathermal climate. *Adv. Atmos. Sci.,* **17,** 445–457.

——, 2002: The mid-Holocene climate simulated by a grid-point AGCM coupled with a biome model. *Adv. Atmos. Sci.,* **19,** 205–218.

Wang, H. Y., H. Y. Liu, H. T. Cui, and N. Abrahamsen, 2001: Terminal Pleistocene/Holocene palaeoenvironmental changes revealed by mineral-magnetism measurements of lake sediments for Dali Nor area, southeastern Inner Mongolia Plateau, China. *Palaeogeogr. Palaeoclimatol. Palaeoecol.,* **170,** 115–132.

Wang, J. Q., and J. L. Liu, 2001: The records of amino acids and organic carbon isotope for Holocene megathermal in Changbaishan area (in Chinese). *Acta Micropalaeontol. Sin.,* **18,** 392–398.

Wang, S. Y., H. Y. Lü, J. Q. Liu, and J. F. W. Negendank, 2007: The early Holocene optimum inferred from a high-resolution pollen record of Huguangyan Maar Lake in southern China. *Chin. Sci. Bull.,* **52,** 2829–2836.

Wang, T., H. J. Wang, and D. Jiang, 2010: Mid-Holocene East Asian summer climate as simulated by the PMIP2 models. *Palaeogeogr. Palaeoclimatol. Palaeoecol.,* **288,** 93–102.

Wei, J. F., and H. J. Wang, 2004: A possible role of solar radiation and ocean in the mid-Holocene East Asian monsoon climate. *Adv. Atmos. Sci.,* **21,** 1–12.

Wei, K. Q., and R. F. Lin, 1994: An enquiry into palaeoclimatic information from oxygen isotopic profile of Dunde ice core in Qilianshan (in Chinese). *Geochimica,* **23,** 311–320.

Wen, R. L., J. L. Xiao, Z. G. Chang, D. Y. Zhai, L. Zhou, Q. H. Xu, Y. C. Li, and S. Itoh, 2010: Holocene vegetation and climate changes reflected by the pollen record of Hulun Lake, north eastern Inner Mongolia (in Chinese). *Quat. Sci.,* **30,** 1105–1115.

Wu, J. L., S. M. Wang, and H. D. Wang, 1996: Characters of the evolution of climate and environment of Holocene in Aibi Lake basin in Xinjiang (in Chinese). *Oceanol. Limnol. Sin.,* **27,** 524–530.

Wu, Y., A. Lücke, B. Wünnemann, S. Li, and S. Wang, 2007: Holocene climate change in the central Tibetan Plateau inferred by lacustrine sediment geochemical records. *Sci. China,* **50D,** 1548–1555.

Xiao, J. Y., H. B. Lü, W. J. Zhou, Z. J. Zhao, and R. H. Hao, 2007: Evolution of vegetation and climate since the last glacial maximum recorded at Dahu peat site, South China. *Sci. China,* **50D,** 1209–1217.

Xu, Q. H., S. Y. Chen, Z. C. Kong, and N. Q. Du, 1988: Preliminary discussion of vegetation succession and climatic change since the Holocene in the Baiyangdian Lake district. *Acta Phytoecol. Geobotan. Sin.* (in Chinese). **12,** 143–151.

——, J. L. Xiao, N. Toshio, X. L. Yang, Z. J. Yang, W. D. Liang, I. Biro, and S. Y. Yang, 2003: Quantitative reconstructed climatic changes of Daihai Basin by pollen data (in Chinese). *Mar. Geol. Quat. Geol.,* **23,** 99–108.

Xue, J. B., and W. Zhong, 2008: Holocene climate change recorded by lacustrine sediments in Barkol Lake and its regional comparison (in Chinese). *Quat. Sci.,* **28,** 610–620.

Yang, X. D., S. M. Wang, B. Xue, and G. B. Tong, 1995: Vegetational development and environmental changes in Hulun Lake since late Pleistocene (in Chinese). *Acta Palaeontol. Sin.,* **34,** 647–656.

——, Y. X. Zhu, X. Z. Jiang, Y. H. Wu, and S. M. Wang, 1998: Environmental changes from spore-pollen record of Mianyang region over the past 10000 years (in Chinese). *J. Lake Sci.,* **10,** 23–29.

Yang, Y. X., and S. Y. Wang, 2002: Study on mire development and palaeoenvironment change since 9.0 ka B.P. in the east part of the Xiaoxinganling Mountains (in Chinese). *J. Mountain Sci.,* **20,** 129–134.

——, and ——, 2003: Study on mire development and paleoenvironment change since 8.0 ka B.P. in the northern part of the Sanjiang Plain (in Chinese). *Sci. Geogr. Sin.,* **23,** 32–38.

Yao, T. D., L. G. Thompson, Y. F. Shi, D. H. Qin, K. Q. Jiao, Z. H. Yang, L. D. Tian, and E. M. Thompson, 1997: Climate variation since the Last Interglaciation recorded in the Guliya ice core. *Sci. China,* **40D,** 662–668.

Yu, C. X., Y. L. Luo, and X. J. Sun, 2008: A high-resolution pollen records from Ha'ni Lake, Jilin, northeast China showing climate changes between 13.1 cal. ka B. P. and 4.5 cal. ka B.P (in Chinese). *Quat. Sci.,* **28,** 929–938.

Yu, G., I. C. Prentice, S. P. Harrison, and X. Sun, 1998: Pollen-based biome reconstructions for China at 0 and 6000 years. *J. Biogeogr.,* **25,** 1055–1069.

——, and Coauthors, 2000: Palaeovegetation of China: A pollen data-based synthesis for the mid-Holocene and last glacial maximum. *J. Biogeogr.,* **27,** 635–664.

Zhai, Q. M., W. L. Qiu, R. Q. Li, Y. Zhao, and L. M. Zheng, 2000: The middle and late Holocene lacustrine sediments and its climate significance of Angulinao–Bojianghaizi Lakes, Inner Mongolia (in Chinese). *J. Palaeogeogr.,* **2,** 84–91.

Zhang, H. C., Y. Z. Ma, B. Wünnemann, and H.-J. Pachur, 2000b: A Holocene climatic record from arid northwestern China. *Palaeogeogr. Palaeoclimatol. Palaeoecol.,* **162,** 389–401.

Zhang, H. L., J. M. Qin, Y. S. Lin, X. Q. Pu, and C. H. Liu, 2009: A study on climate change pattern of the middle Holocene in Xundian, Yunnan (in Chinese). *Trop. Geogr.,* **29,** 515–519.

Zhang, J. H., and Z. C. Kong, 1999: Study on vegetation and climate changes in Beijing region since late Pleistocene. *Chin. Geogr. Sci.,* **9,** 243–249.

Zhang, M. L., D. X. Yuan, Y. S. Lin, J. M. Qin, C. Zhang, and H. Cheng, 2003: High resolution climatic records of stalagmite from Xiangshui Cave in Guilin since 6.00 ka B P (in Chinese). *Acta Geosci. Sin.,* **24,** 439–444.

——, H. Cheng, Y. S. Lin, J. M. Qin, H. L. Zhang, L. L. Tu, H. Wang, and Y. M. Feng, 2004: High resolution paleoclimatic environment records from a stalagmite of Dongge Cave since 15,000 a in Libo, Guizhou Province, China (in Chinese). *Geochimica,* **33,** 65–74.

Zhang, Q., H. S. Sundqvist, A. Moberg, H. Körnich, J. Nilsson, and K. Holmgren, 2010: Climate change between the mid and late Holocene in northern high latitudes—Part 2: Model–data comparisons. *Climate Past,* **6,** 609–626.

Zhang, Y. L., 2006: Palynological assemblages and palaeovegetation and palaeoclimate of the Holocene in eastern Shanghai (in Chinese). *J. Palaeogeogr.,* **8,** 35–41.

Zhang, Z. K., R. J. Wu, S. M. Wang, J. Shen, Y. H. Wu, and S. F. Li, 2000a: Environmental evolution recorded by lake sediments from Erhai Lake, Yunnan Province in Holocene megathermal (in Chinese). *Oceanol. Limnol. Sin.,* **31,** 210–214.

Zhao, H. Y., X. T. Leng, and S. Z. Wang, 2002: Distribution, accumulation rate of peat in the Changbaishan Mountains and climate change in Holocene (in Chinese). *J. Mountain Sci.,* **20,** 513–518.

Zhao, X. T., L. Y. Tang, C. M. Shen, and S. H. Wang, 1994: Holocene climate change and coastal evolution in Qingfeng Section, Jianhu County, Jiangsu Province (in Chinese). *Acta Oceanol. Sin.,* **16,** 78–88.

Zheng, W., and Y. Yu, 2009: The Asian monsoon system of the mid-Holocene simulated by a coupled GCM (in Chinese). *Quat. Sci.,* **29,** 1135–1145.

Zheng, Y. Q., G. Yu, S. M. Wang, B. Xue, D. Q. Zhuo, X. M. Zeng, and H. Q. Liu, 2004: Simulation of paleoclimate over East Asia at 6 ka BP and 21 ka BP by a regional climate model. *Climate Dyn.,* **23,** 513–529.

Zheng, Z., 1990: Holocene pollen analysis and environmental research in the Chaoshan Plain (in Chinese). *Trop. Oceanol.,* **9,** 31–38.

Zhong, W., and Q. Shu, 2001: Palaeoclimatic and palaeohydrologic oscillations since about 12.0 ka B.P. at Bosten Lake, southern Xinjiang (in Chinese). *Oceanol. Limnol. Sin.,* **32,** 213–220.

Zhou, B., and P. Zhao, 2009: Inverse correlation between ancient winter and summer monsoons in East Asia? *Chin. Sci. Bull.,* **54,** 3760–3767.

Zhou, W. J., Z. S. An, and M. J. Head, 1994: Stratigraphic division of Holocene loess in China. *Radiocarbon,* **36,** 37–45.

——, X. F. Yu, A. J. T. Jull, G. Burr, J. Y. Xiao, X. F. Lu, and F. Xian, 2004: High-resolution evidence from southern China of an early Holocene optimum and a mid-Holocene dry event during the past 18,000 years. *Quat. Res.,* **62,** 39–48.

Zhu, L. P., and Coauthors, 2007: Environmental changes reflected by core sediments since 8.4 ka in Nam Co, central Tibet of China (in Chinese). *Quat. Sci.,* **27,** 588–597.